

Numerical simulation of multilayer cellular scaffolds with 3D and 1D elements

Hamid Reza Khanaki¹, Sadegh Rahmati^{2, *}, Mohammad Nikkhoo³,
Mohammad Haghpanahi⁴, Javad Akbari⁵

^{1,2}Department of Mechanical Engineering, Science and Research Branch, Islamic Azad University, Tehran, Iran

³ Department of Biomedical Engineering, Science and Research Branch, Islamic Azad University, Tehran, Iran

E-mail: khanaki.hamid@gmail.com, srahmati@srbiau.ac.ir, m.nikkhoo@srbiau.ac.ir

⁴Biomechanics Group, Department of Mechanical Engineering, Iran University of Science and Technology, Tehran, Iran

⁵Department of Mechanical Engineering, Sharif University of Technology, Tehran, Iran

E-mail: mhaghpanahi@iust.ac.ir, akbari@sharif.edu

*Corresponding author

Received: 7 July 2020, Revised: 1 October 2020, Accepted: 1 December 2020

Abstract: In this paper, an attempt has been made to provide a numerical method for investigating the mechanical properties of multilayer scaffolding. These scaffolds can be used as implants in bone fractures. For this purpose two numerical simulation methods are introduced to predict the elastic properties of multilayer cell scaffolds. These simulations are based on two models: a 3D model with a volumetric element, and a 1D model with a linear element. To compare the results of these models, three types of two- and three-layer titanium alloy scaffolds have been simulated by the two methods. Also, Young's modulus of the scaffolds has been compared with the experimental conclusions of earlier studies. The results confirm that simulations with 1D models are more cost-effective compared to 3D ones. Additionally, because of the more reliable agreement of Young's modulus results of numerical modeling with the linear element (1.8 to 5 times) compared to the volumetric element (11 to 23 times) compared to the experimental findings, the numerical method with the linear elements can be a reliable tool for studying multilayer scaffoldings.

Keywords: Additive Manufacturing, Finite Element Modeling, Multilayer scaffold, Numerical analysis, Open-lattice cellular scaffold

Reference: Hamid Reza Khanaki, Sadegh Rahmati, Mohammad Nikkhoo, Mohammad Haghpanahi, and Javad Akbari, "Numerical simulation of multilayer cellular scaffolds with 3D and 1D elements", Int J of Advanced Design and Manufacturing Technology, 2020, Vol. 13/No. 4, pp. 39-47. DOI: 10.30495/admt.2020.1905314.1207

Biographical notes: **Hamid Reza Khanaki** is a PhD student of Mechanical Engineering from University of IAU, Science and Research Branch. He is currently Instructor at the Technical and Vocational College, IAU University, Tehran Sama Branch. His current research interest includes Finite Element Analysis and Additive Manufacturing. **Sadegh Rahmati** received his PhD in Additive Manufacturing Technology from Nottingham University in 1999. He is currently Associate Professor at the Department of Medical Science and Technology, IAU University, Science and Research Branch. His current research interest includes Medical Additive Manufacturing and Biomedical Engineering. **Mohammad Nikkhoo** received his PhD in Biomechanical Engineering from University of Science and Technology in 2013. He is currently Assistant Professor at the Department of Medical Science and Technology, IAU University, Science and Research Branch. His current research interest includes Orthopaedic Biomechanics and Finite Element Analysis. **Mohammad Haghpanahi** received his PhD in Biomechanical Engineering from ENSAM University, Paris in 1985. He is currently Professor of Biomedical Engineering at the University of Science and Technology. His current research interest includes Orthopaedic Biomechanics and Finite Element Analysis. **Javad Akbari** received his PhD in Mechanical Engineering from Chiba University, Japan in 1993. He is currently Associate Professor of Mechanical engineering at the Sharif University of Technology. His current research interest includes Machining, Grinding, Ultrasonic and Additive Manufacturing.

1 INTRODUCTION

One of the innovative methods used in orthopaedics is based on the design of metallic bone scaffolds and the implants which imitates the natural structure of the host bones [1]. Proper design of the scaffolds structure is considered as a key factor for satisfied clinical outcomes. An ideal metallic implant, similar to natural bone, should have sufficient porosity to some extent and have parts with controlled directional properties. Despite recent advances in biological materials, the design and construction of such scaffolds is still a challenge [2]. The scaffolds for bone implants should be of high strength against external loading and, in addition, Young's modulus should be similar to the neighboring tissue properties of the implant to avoid the protective effect of stress shielding and bone resorption [3]

Recently, due to the appearance and maturity of the additive manufacturing technology that has provided the possibility of manufacturing of arbitrarily complex shapes in the micro [4] and even nanoscale [5, 6], the interest in the manufacturing of cellular scaffolds with proper mechanical properties have been increased. The mechanical properties of open-lattice cellular scaffolds are basically dependent on the ingredient materials' selection, structure density, shape, and geometry of the unit cell that results in the selection of diverse mechanical properties of the structure. The open-lattice cellular scaffolds can be constructed from long and slim beams (truss) that usually could be in any profiles including circular [7, 8], square [9, 10], rectangular, I-beam or hollow [11, 12].

The scaffolds can be regulated in many different configurations depending on the intended application. Cube [13]–[15], truncated cube [16], rhombic dodecahedron [17], [18]–[21], truncated cuboctahedron [22], Kelvin cell [23, 24], rhombicuboctahedron [25], three dimensional Kagome [26], pyramidal [27], diamond [17, 28, 29], and truncated octahedron [30]–[32] are the open-lattice cellular morphologies that have been mostly studied. The mechanical properties of lattice structures are dependent on the number of layers in addition to the structure density, shape and geometry of the unit cell. Therefore, the unit cell shape, dimensions and number of layers could be changed to optimize the mechanical properties. A multi-layer scaffold with a repetitive unit cell for structures that are particularly used in bio-medicine applications has been recently discussed by experimental [2], analytical, and numerical methods [33].

In this researches, the double-layer and three-layer titanium (Ti6Al4V) scaffolds have been compared. This research showed that the titanium scaffolds with graded porosity, besides the decrease of Young's modulus

compared to the dense alloy, had significant formability [2]. The optimal design of porous scaffolds requires tools that can be used to predict the mechanical properties of any set of design parameters. There are three methods such as experimental, numerical and analytical that can be used to predict the mechanical properties of porous biomaterials.

The experimental approach is probably a more precise approach, but it requires the fabrication and mechanical testing of a large number of samples [34]. performing large number of experimental tests on cellular structures can be time consuming and expensive. In order to investigate further scaffold designs by variation of the geometrical parameters, a numerical approach should be used, based on target values to optimize mechanical properties. Finite element (FA) analysis offers the possibility to investigate the mechanical properties like structural modulus, compressive strength and stress distribution within complex structures to optimize the requirements for the field of clinical application without the use of scaffold fabrication or destructive experimental testing [35].

Most of the researches have been conducted on the ordered homogeneous porosities based on the unit cell repetition and the multi-layer scaffolds' researches have been less studied. The effect of element type on the results of numerical simulation of multilayer cell scaffolds has not been investigated so far, which is the purpose of this study. In this paper, multilayer scaffolds are numerically simulated with 1D and 3D elements and the results of mechanical properties of scaffolds under uniaxial compress load are compared with experimental results.

2 RESEARCH METHODOLOGY

It has been shown that changes in Young's modulus of cubic scaffolds with cell dimensions of $3 \times 3 \times 3$ and higher have an approximately linear behavior in regular cell scaffolds with BCC and diamond unit cells. These changes were around 1 to 5% for scaffolds with $5 \times 5 \times 5$ cell dimensions compared to $7 \times 7 \times 7$ ones for different unit cell sizes [33]. Hence, in regular cell scaffolds, numerical simulation of a confined number of cube scaffolds can express the mechanical properties of extremely large scaffolds. Thus, there is a mismatch at the boundary of the layers in multi-layer scaffolds owing to the difference in the porosity of the layers. This mismatch is not the same at various heights. Accordingly, the only simplification requisite in the numerical simulation of multilayer cell scaffolds will be the geometric frame of the scaffold. In this research, to validate the correctness of numerical approaches, three

types of two-layer cylindrical scaffolding (outer diameter 15 mm and length 35 mm) with a diameter of 0.5 mm strut of titanium alloy under compressive load based on available information from previous research were studied by two numerical methods with a volumetric element and linear element using ANSYS software “Fig. 1”. The mechanical characteristics of scaffolds were determined by doing uniform compression test simulations and compared with experimental results. Furthermore, since the examination was in the entirely elastic region, it was assumed that the elastic material was linear.

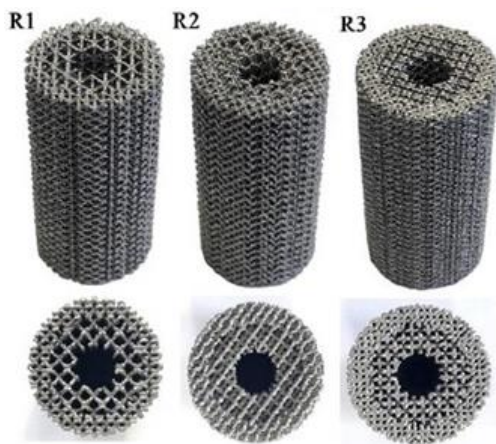


Fig. 1 Samples of two-layer scaffolds formed by the EBM method [2].

Table 1 Design and geometric parameter of scaffolds [2].

| Scaffold | Inner diameter (5 mm) | Middle diameter (11 mm) | Outer diameter (15 mm) | Porosity % |
|----------|-----------------------|-------------------------|------------------------|------------|
| R1-B | Open hole | BCC-2 | BCC-1.25 | 64 |
| R2-D | Open hole | D-2 | D-1.25 | 65 |
| R3-B | Open hole | BCC-1.25 | BCC-1 | 22 |

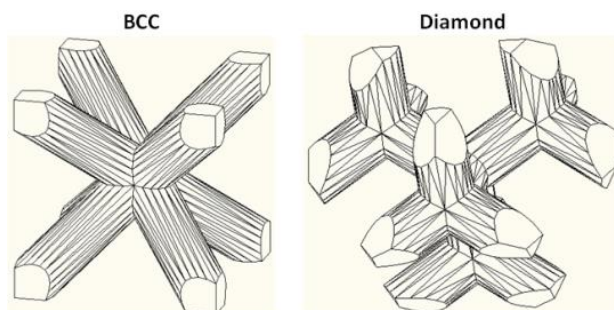


Fig. 2 BCC (left) and diamond (right) scaffold cell units.

“Table.1” gives the geometric parameters of the simulated scaffolds, and “Fig. 2” gives the form of the unit cells of the specified scaffolds. In “Table.1”, the first letter of the unit cell name is used next to the name of the scaffold, the letter B for the BCC unit cell and the letter D for the Diamond unit cell. The mechanical properties of titanium alloy (Ti6Al4V) used in the simulations are listed in “Table. 2”.

Table 2 Mechanical properties of titanium alloy [2].

| Properties | Symbol | Value |
|-----------------|------------|---------|
| Young’s modulus | E_s | 114 GPa |
| Poisson’s ratio | N_s | 0.37 |
| Yield strength | σ_y | 920 MPa |

2.1. Modeling

3D volumetric model and linear model were designed in AutoCAD software. Also, in the volumetric model, 1/8 of the total scaffold was modeled “Fig. 3” to decrease the calculation time according to the symmetry of the scaffold.

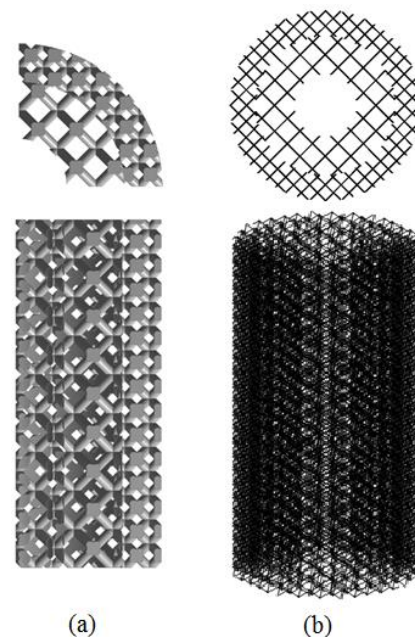


Fig. 3 Scaffolding: R1-B (a): volumetric model, (b): linear model.

Also, in both models, the analysis was considered static. Furthermore, since the analysis was in the fully elastic region, the behavior of the scaffold material in the software was considered linear elastic.

2.2. Simulation with the volumetric element

After loading model in the software, volumetric elements were used for meshing “Fig. 4”. The nodes on the three planes $xy (z = 0)$, $yz (x = 0)$, and $zx (y = 0)$ are restricted to move along each plane to apply the boundary conditions, as shown in “Fig. 5”. Proper

rotational conditions are set to evaluate symmetry. Further, the nodes in contact with the top plane were free to move along the surface and were limited for the symmetry of all rotations of these nodes.

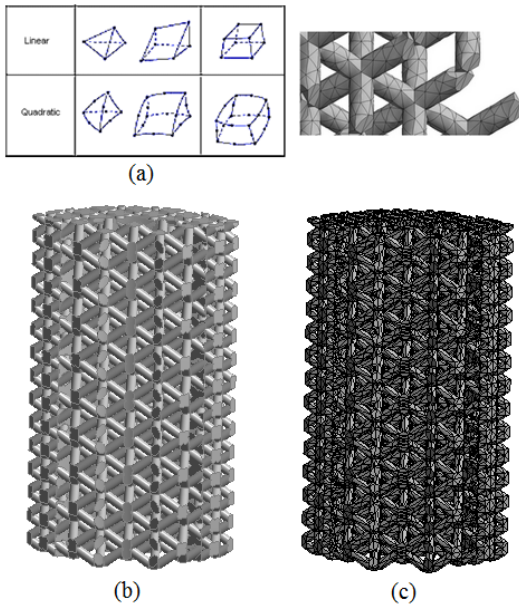


Fig. 4 (a): Volumetric element [36], and (b): model (c): meshed model.

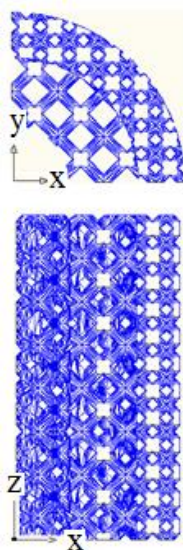


Fig. 5 Directions of scaffold volumetric model planes.

After setting the boundary conditions, the processing operation is performed, and the force and displacement values are computed. Then, the axial stress of the scaffold is obtained by dividing the axial force by the cross-section of the scaffold. Likewise, the axial strain is obtained by dividing the amount of compression by the height of the scaffold. Then, the elastic modulus is

obtained by dividing the applied axial stress by the resulting axial strain.

2.3. Simulations with the linear element

Linear elements are normally more cost-effective than the surface and volumetric elements. By using linear elements, organizing and analyzing large porous compositions consisting of many struts does not need much computational effort [37]. Accordingly, first, the spatial model of the axes of rod structures, the same as the porous structures of the present research, is entirely illustrated with AutoCAD software. Then, in Ensis software, the cross-section of the struts is created, and the vertices are connected “Fig. 6”.

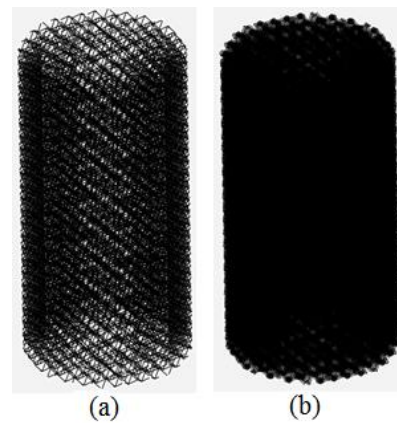


Fig. 6 The spatial model of scaffolding struts (a): before and (b): after forming the cross-section of the struts.

| | | |
|-----------|--|-------------|
| Linear | | Beam, Truss |
| Quadratic | | Beam |
| Cubic | | Beam |

(a)

(b)

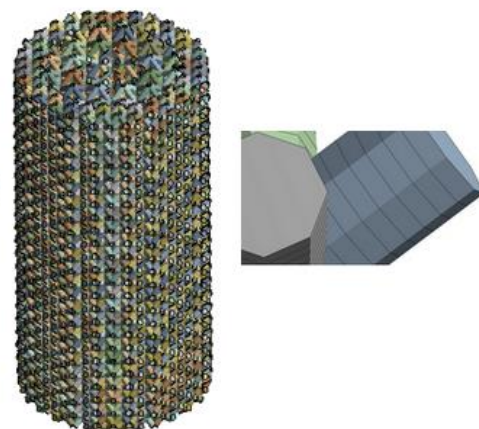


Fig. 7 Linear element [36], and the meshed model space.

Since the struts of open-network cell formations are usually affected by axial and flexural loads, two- or three-node beam components can be considered as the most suitable choice for this idea through program control “Fig. 7”.

After simulating the samples, to apply the boundary conditions, the nodes at the top of the scaffold are moved in the direction of the scaffold axis, such that the porous construction moves to a certain compressive strain. Additionally, in all simulated porous structures, to decrease the impact of boundary conditions on the mechanical characteristics of the scaffold, the nodes at the bottom plate of the network structure were limited in three directions ($x, y, z = 0$). The axial stress of the scaffold was achieved by dividing the axial force by the cross-section of the scaffold. Likewise, the axial strain was obtained by dividing the compression by the height of the scaffold. Next, the elastic modulus was obtained by dividing the applied axial stress by the obtained axial strain. By achieving the maximum stress in the porous structure and then comparing it with the yield stress of titanium alloy, the yield strain of the porous structure was obtained. Then, by multiplying this yield stress in Young’s modulus of the scaffold, the yield stress of the scaffold is determined. Numerical simulation of multilayer scaffolds was performed with a linear element and showed that Young’s modulus and yield stress in the scaffolds with constant porosity were related to a unit-cell and the two-layer scaffolds, without changing Young’s modulus, had higher yield stress [38].

3 RESULTS AND DISCUSSION

3.1. Simulation with the volumetric element

“Fig. 8” presents the stress-strain curve of scaffolding R1-B achieved by the volumetric element simulation method.

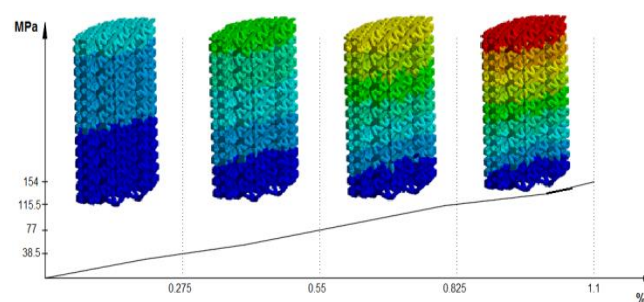


Fig. 8 Stress-strain curve of R1-B scaffolding with the volumetric element.

“Fig. 9” displays the Von Mises stress obtained by volumetric simulation of R1-B scaffolding. It also shows that the maximum stress forms at the layer boundary.

3.2. Simulations with the linear element

“Fig. 10” gives the force and displacement curve of the R1-B scaffolding, obtained by the linear element simulation method after 2 mm compression.

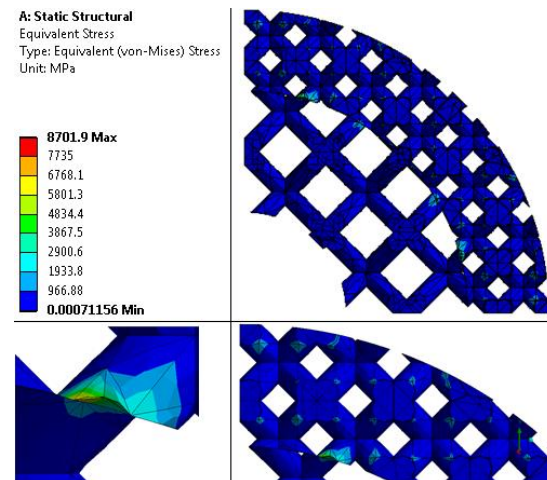


Fig. 9 von Mises stress of the R1-B scaffolding with the volumetric element.

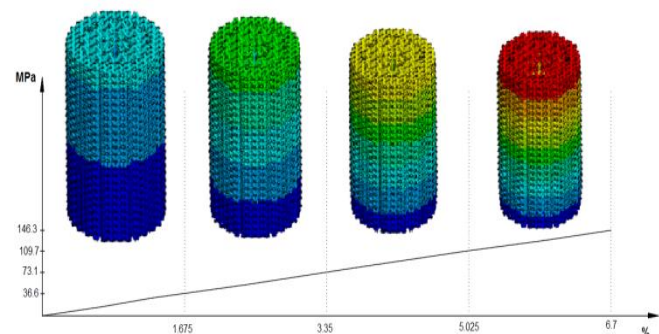


Fig. 10 Stress-strain curve of the R1-B scaffolding with the linear element.

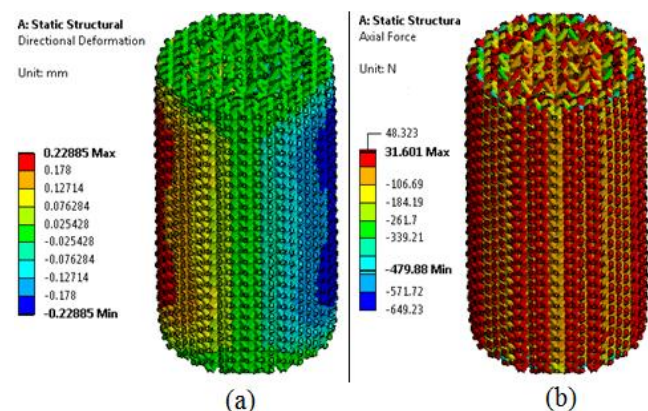


Fig. 11 (a): Radial displacement of unit cell nodes, (b): Axial force of unit cell struts of the R1-B scaffolding with the linear element.

Next, the radial displacement of unit cell nodes “Fig. 11-a” and the axial force of unit cell struts “Fig. 11-b” are presented by linear simulation of the obtained R1-B scaffolding. Using the radial displacement of the nodes, the deformation of the scaffold will be apparent after loading. Also, by dividing the force of the unit cell struts by the cross-section of the strut forming the unit cell, the axial stress of the strut after loading can be calculated. By comparing this stress with the yield stress of the material forming the scaffold, the yield stress of the scaffold can be estimated.

3.3. Comparison of simulation with volumetric and linear elements

Because of the increase in the number of components in the simulation with volumetric elements, and the significant increase in calculations, the solution time was much longer than the simulation with linear elements “Table. 3”.

Table 3 Number of scaffolding elements in volumetric and linear modeling methods

| Method | R1-B | | R2-D | | R3-B | |
|-------------------------|-----------------|--------------------|-----------------|--------------------|-----------------|--------------------|
| | Number of nodes | Number of elements | Number of nodes | Number of elements | Number of nodes | Number of elements |
| 1/8 of scaffold FEM(3D) | 70442 | 137808 | 367896 | 667895 | 109117 | 194607 |
| whole scaffold FEM(1D) | 15240 | 24924 | 26892 | 45544 | 34867 | 53776 |
| 3D/1D | 4.62 | 5.53 | 13.68 | 14.66 | 3.13 | 3.62 |

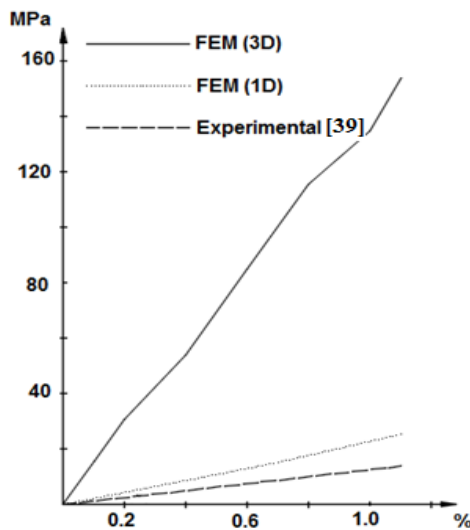


Fig. 12 stress-strain curve of linear, volumetric, and experimental simulation of R1-B scaffolding.

The stress-strain curve of linear, volumetric, and experimental simulation of R1-B scaffolding in “Fig. 12” confirms that Young’s modulus of the numerical

method with linear element is (2.26 GPa) 1.8 times that of Young’s modulus of the experimental model (1.25 GPa). But this ratio was about 11 times for the volumetric element (13.9 GPa).

“Fig. 13” gives a comparison of Young’s modulus of the three scaffolds studied. In the simulation with volumetric elements, the results are significantly different from the experimental method. This is because of the stiffness of the nodes at the vertices and the surrounding. The difference between these results in terms of the ratio of strut diameter to cell size (d / L) for the constant diameter (d) of the strut reveals that, for large d / L , the density is higher and for small d / L , the density is lower.

Also, “Fig. 13” shows a better agreement in the results for Young’s modulus of numerical modeling with the linear element (1.8 to 5 times) compared to the experimental findings with the volumetric element (11 to 23 times).

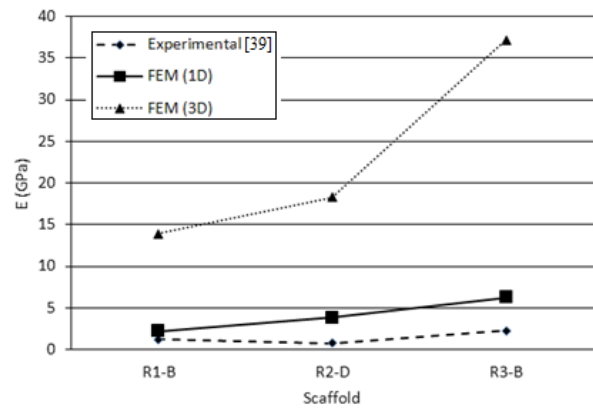


Fig. 13 Comparison of Young’s modulus of simulated models for volumetric, linear and experimental elements.

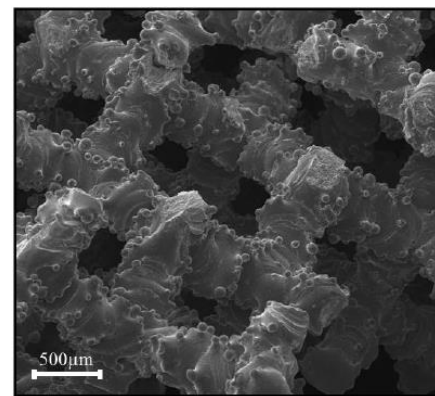


Fig. 14 Scanning electron microscope image of R2 scaffolding after the complete break [2].

The low values of Young’s modulus in the experimental simulation are due to production defects; Such as the

presence of free bonds and powder particles with incomplete melting in the scanning electron microscope image obtained after the complete break “Fig. 14”. Furthermore, the reduction in Young modulus of R2-D scaffolding compared to R1-B scaffolding in the experimental results is owing to the increase in the number of nodes in diamond-shaped cells compared to BCC cells, and the addition in the formation defects. However, the same behavior of Young's modulus yields numerical modeling with the linear element, and the experimental method can show that the numerical method with the linear elements can be a proper tool for research of multilayer scaffolds.

3.4. Young modulus in different heights scaffolds

Due to the relatively linear behavior of Young's modulus changes for a height of three cells and higher in regular scaffolds, to study the effect of scaffold height on Young's modulus of multilayer scaffolding, in the linear element simulation method, the considered scaffolds with a height of 15 mm were as well simulated. The comparison of these results with the results with 35mm scaffolding (“Table. 4” and “Fig. 15”) reveals an approximate similarity (1-5%). Therefore, to reduce the solution time in the numerical method, scaffolds with shorter heights can be used. According to the comparison of the results of regular scaffolding, the height of the scaffold suitable for the numerical method equals the height of 5 units of the largest cells constituting the scaffold.

Table 4 Numerical results of young modulus in different scaffolds heights

| Height (mm) | R1-B (GPa) | R2-D (GPa) | R3-B (GPa) |
|-------------|------------|------------|------------|
| 15 | 2.22 | 4.47 | 6.57 |
| 35 | 2.18 | 4.34 | 6.28 |

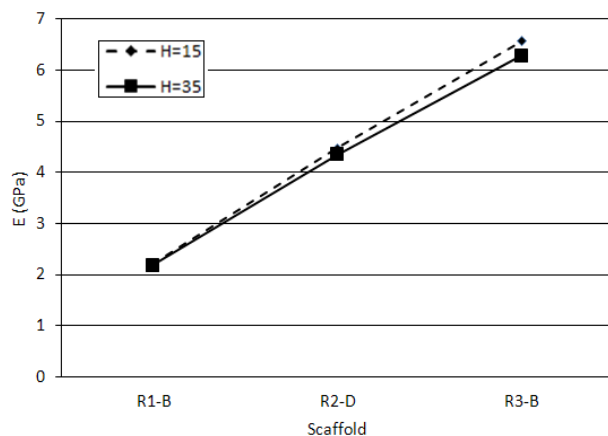


Fig. 15 Comparison of numerical results of Young's modulus of scaffolds with several heights.

4 CONCLUSION

The comparison of numerical simulations of multilayer scaffolds with three-dimensional and one-dimensional models in Ansis software and the findings of experimental experiments revealed, simulations with one-dimensional models are more cost-effective compared to three-dimensional ones. Using a one-dimensional model, the creation and analysis of large porous structures with many struts do not need much computational work. Additionally, because of the more reliable agreement of Young's modulus results of numerical modeling with the linear element (1.8 to 5 times) compared to the volumetric element (11 to 23 times) compared to the experimental findings, and the same behavior of Young's modulus results for different scaffolds in numerical modeling with the linear element and experimental method, the numerical method with the linear elements can be a reliable tool for studying multilayer scaffoldings.

REFERENCES

- [1] Wang, X., Xu, S., Zhou, S., Xu, W., Leary, M., Choong, P., Qian, M., Brandt, M. and Xie, Y. M., Topological design and additive manufacturing of porous metals for bone scaffolds and orthopaedic implants: a review, *Biomaterials*, Vol. 83, No. 5, 2016, pp. 127-141.
- [2] Surmeneva, M., Surmenev, R., Chudinova, E., Koptioug, A., Tkachev, M., Gorodzha, S. and Rannar, L. E., Fabrication of multiple-layered gradient cellular metal scaffold via electron beam melting for segmental bone reconstruction, *Materials & Design*, Vol. 133, No. 5, 2017, pp. 195–204.
- [3] Laurencin, C. T., Khan, Y., Ma, P. X. and Elisseeff, J., Polymer/Calcium Phosphate Scaffolds for Bone Tissue Engineering, In: Ma, P. X., Elisseeff, J. (eds) *Scaffolding in tissue engineering*, 2005, pp. 253–265.
- [4] Vaezi, M., Seitz, H., and Yang, S., A review on 3D micro-additive manufacturing technologies, *The International Journal of Advanced Manufacturing Technology*, Vol. 67, No. 5-8, 2013, pp. 1721–1754.
- [5] Ahn, S., Chun, D., and Kim, C., Nanoscale hybrid manufacturing process by nano particle deposition system (NPDS) and focused ion beam (FIB), *CIRP Annals-Manufacturing Technology*, Vol. 60, No. 1, 2011, pp. 583–586.
- [6] Petrochenko, P. E., Torgersen, J., Gruber, P., Hicks, L. A., Zheng, J., Kumar, G., Narayan, R.J., Goering, P.L., Liska, R., and Stampfl, J., *Laser 3D Printing with Sub-Microscale Resolution of Porous Elastomeric Scaffolds for Supporting Human Bone Stem Cells*, *Advanced healthcare materials*, Vol. 4, No. 5, 2014, pp. 739–747.
- [7] Deshpande, V. S., and Fleck, N. A., Collapse of truss core sandwich beams in 3-point bending, *International Journal*

- of Solids and Structures, Vol. 38, No. 36-37, 2001, pp. 6275–6305.
- [8] Wang, J., Evans, A. G., Dharmasena, K., et al., On the performance of truss panels with Kagome cores, *International Journal of Solids and Structures*, Vol. 40, No. 25, 2003, pp. 6981–6988.
- [9] Kooistra, G. W., Deshpande, V. S., and Wadley, H. N. G., Compressive behavior of age hardenable tetrahedral lattice truss structures made from aluminium, *Acta Materialia*, Vol. 52, No. 14, 2004, pp. 4229–4237.
- [10] Rathbun, H. J., Wei, Z., He, M. Y., et al., Measurement and simulation of the performance of a lightweight metallic sandwich structure with a tetrahedral truss core, *Journal Applied Mechanics*, Vol. 71, No. 3, 2004, pp. 368–374.
- [11] Queheillalt, D. T., and Wadley, H. N. G., Cellular material lattices with hollow trusses, *Acta Materialia*, Vol. 53, No. 2, 2005, pp. 303–313.
- [12] Queheillalt, D. T., and Wadley, H. N. G., Pyramidal lattice truss structures with hollow trusses, *Materials Science Engineering: A*, Vol. 397, No. 1-2, 2005, pp. 132–137.
- [13] Gibson, L. J., and Ashby, M. F., *Cellular solids: structure and properties*. Cambridge university press, 1997.
- [14] Luxner, M. H., Woesz, A., Stampfl, J., Fratzl, P., and Pettermann, H. E., A finite element study on the effects of disorder in cellular structures, *Acta biomaterialia*, Vol. 5, No. 1, 2009, pp. 381–390.
- [15] Parthasarathy, J., Starly, B., Raman, S., and Christensen, A., Mechanical evaluation of porous titanium (Ti6Al4V) structures with electron beam melting (EBM), *Journal of the mechanical behavior of biomedical materials*, Vol. 3, No. 3, 2010, pp. 249–259.
- [16] Hedayati, R., Sadighi, M., Mohammadi-Aghdam, M., and Zadpoor, A. A., Mechanical properties of regular porous biomaterials made from truncated cube repeating unit cells: analytical solutions and computational models, *Materials Science and Engineering: C*, Vol. 60, 2016, pp. 163–183.
- [17] Campoli, G., Borleffs, M., Yavari, S. A., Wauthle, R., Weinans, H., and Zadpoor, A. A., Mechanical properties of open-cell metallic biomaterials manufactured using additive manufacturing. *Materials and Design*, Vol. 49, 2013, pp. 957–965.
- [18] Babaee, S., Jahromi, B. H., Ajdari, A., Nayeb-Hashemi, H., and Vaziri, A., Mechanical properties of open-cell rhombic dodecahedron cellular structures, *Acta Materialia*, Vol. 60, No. 6, 2012, pp. 2873–2885.
- [19] Borleffs, M., Finite element modeling to predict bulk mechanical properties of 3D printed metal foams, TU Delft, Delft University of Technology, 2012.
- [20] Shulmeister, V., Van der Burg, M., Van der Giessen, E., and Marissen, R., A numerical study of large deformations of low-density elastomeric open-cell foams, *Mechanics of materials*, Vol. 30, No. 2, 1998, pp. 125–140.
- [21] Hedayati, R., Hosseini-Toudeshky, H., Sadighi, M., Mohammadi-Aghdam, M., Zadpoor, A. A., Computational prediction of the fatigue behavior of additively manufactured porous metallic biomaterials, *International Journal of Fatigue*, Vol. 84, 2016, pp. 67–79.
- [22] Hedayati, R., Sadighi, M., Mohammadi-Aghdam, M., and Zadpoor, A. A., Mechanical behavior of additively manufactured porous biomaterials made from truncated cuboctahedron unit cells. *International Journal of Mechanical Sciences*, Vol. 106, 2016, pp. 19–38.
- [23] Warren, W., Kraynik, A., Linear elastic behavior of a low-density Kelvin foam with open cells, *Journal of Applied Mechanics*, Vol. 64, 1997, pp. 787–794.
- [24] Zheng, X., Lee, H., Weisgraber, T. H., Shusteff, M., DeOtte, J., Duoss, E. B., Kuntz, J. D., Biener, M. M., Ge, Q., Jackson, J. A., Ultralight, ultrastiff mechanical metamaterials, *Science*, Vol. 344, 2014, pp. 1373–1377.
- [25] Hedayati, R., Sadighi, M., Mohammadi-Aghdam, M., Zadpoor, A. A., Mechanics of additively manufactured porous biomaterials based on the rhombicuboctahedron unit cell, *Journal of the Mechanical Behavior of Biomedical Materials*, Vol. 53, 2016, pp. 272–294.
- [26] Ptochos, E., Labeas, G., Elastic modulus and Poisson's ratio determination of microlattice cellular structures by analytical, numerical and homogenisation methods, *Journal of Sandwich Structures and Materials*, Vol. 14, 2012, pp. 597–626.
- [27] Ptochos, E., Labeas, G., Shear modulus determination of cuboid metallic open-lattice cellular structures by analytical, numerical and homogenisation methods, *Journal of Strain*, Vol. 48, 2012, pp. 415–429.
- [28] Hedayati, R., Sadighi, M., Mohammadi-Aghdam, M., Zadpoor, A. A., Mechanics of additively manufactured porous biomaterials based on the rhombicuboctahedron unit cell, *Journal of the Mechanical Behavior of Biomedical Materials*, Vol. 53, 2016, pp. 272–294.
- [29] Ptochos, E., Labeas, G., Elastic modulus and Poisson's ratio determination of microlattice cellular structures by analytical, numerical and homogenisation methods, *Journal of Sandwich Structures and Materials*, Vol. 14, 2012, pp. 597–626.
- [30] Ptochos, E., Labeas, G., Shear modulus determination of cuboid metallic open-lattice cellular structures by analytical, numerical and homogenisation methods, *Journal of Strain*, Vol. 48, 2012, pp. 415–429.
- [31] Ahmadi, S., Campoli, G., Amin Yavari, S., Sajadi, B., Wauthle, R., Schrooten, J., Weinans, H., Zadpoor, A. A., Mechanical behavior of regular open-cell porous biomaterials made of diamond lattice unit cells, *Journal of the Mechanical Behavior of Biomedical Materials*, Vol. 34, 2014, pp. 106–115.
- [32] Hedayati, R., Sadighi, M., Mohammadi-Aghdam, M., Zadpoor, A. A., Effect of mass multiple counting on the elastic properties of open cell regular porous biomaterials, *Materials and Design*, Vol. 89, 2016, pp. 9–20.
- [33] Bitsche, R., Daxner, T., Böhm, H. J., Space-Filling Polyhedra as Mechanical Models for Solidified Dry Foams. *Technische Universität Wien*, 2005.

- [34] Buffel, B., Desplentere, F., Bracke, K., Verpoest, I., Modelling open cell-foams based on the Weaire-Phelan unit cell with a minimal surface energy approach, *International Journal of Solids and Structures*, Vol. 51, 2014, pp. 3461-3470.
- [35] Kraynik, A. M., Reinelt, D. A., Linear elastic behavior of dry soap foams, *Journal of Colloid and interface Science*, Vol. 181, 1996, pp. 511-520.
- [36] Feng, Y. F., Wang, L., Li, X., Ma, Z. S., Zhang, Y., Zhang, Z. Y., and Lei, W., Influence of architecture of β -tricalcium phosphate scaffolds on biological performance in repairing segmental bone defects, *PLoS One*, Vol. 7, No. 11, 2012, e49955.
- [37] Das, A., and Botchwey, E., Evaluation of angiogenesis and osteogenesis, *Tissue Engineering Part B: Reviews*, Vol. 17, No. 6, 2011, pp. 403-414.
- [38] Gérard, C., and Doillon, C. J., Facilitating tissue infiltration and angiogenesis in a tubular collagen scaffold, *Journal of biomedical materials research Part A*, Vol. 93, No. 2, 2010, pp. 615-624.
- [39] Surmeneva, M., Surmenev, R., Chudinova, E., Koptioug, A., Tkachev, M., Gorodzha, S., Rannar, L. E., Fabrication of multiple-layered gradient cellular metal scaffold via electron beam melting for segmental bone reconstruction, *Materials & Design*, 2017; DOI: 10.1016/j.matdes.2017.07.059.
- [40] Khanaki, H. R., Rahmati, S., Nikkhoo, M., Haghpanahi, M., and Akbari, J., Numerical and analytical simulation of multilayer cellular scaffolds, *Journal of the Brazilian Society of Mechanical Sciences and Engineering*, Vol. 42, No. 268, 2020, pp. 1-13.
- [41] Fundamental FEA Concepts and Applications (no data) (https://www.cae.tntech.edu/~chriswilson/FEA/ANSYS/ANSYSguide_fea-concepts.pdf)
- [42] Bandyopadhyay, A., Espana, F., Balla, V. K., Bose, S., Ohgami, Y., and Davies, N. M., Influence of porosity on mechanical properties and in vivo response of Ti6Al4V implants, *Acta Biomaterialia*, Vol. 6, 2010, pp. 1640-1648
- [43] Khanaki, H. R., Rahmati, S., Nikkhoo, M., Haghpanahi, M., and Akbari, J., Numerical Simulation of Homogeneous, Two and Three Lattice Layers Scaffolds with Constant Density, *Journal of Modern Processes in Manufacturing and Production*, Vol. 9, No. 2, 2020, pp. 5-22.